Bistatic mmWave Mapping in Obstructed Environments Using Double-bounce Signals

Ossi Kaltiokallio[†], Yu Ge[⋆], Jukka Talvitie[†], Elizaveta Rastorgueva-Foi[†], Henk Wymeersch[⋆], and Mikko Valkama[†]

[†]Unit of Electrical Engineering, Tampere University, Tampere, Finland
[⋆]Department of Electrical Engineering, Chalmers University of Technology, Göteborg, Sweden

***Abstract*—Integrated sensing and communication is envisioned to play a pivotal role in future 6G system, enabling various sensing tasks including positioning and mapping. In a bistatic scenario, sensing relies on non-line-of-sight signals that interact with objects in the surrounding environment. Prior works typically assume first-order interactions, meaning that the signal only interacts once with a single object in the environment. In this paper, we investigate the use of higher-order interactions for mapping the environment using mmWave signals. We devise and demonstrate a novel mapping method, based on the position and landmark estimates of an existing snapshot simultaneous localization and mapping algorithm, using double-bounce signals.**

***Index Terms*—ISAC, 5G/6G, mmWave, multi-bounce propagation, bistatic mapping**

I. Introduction

The use of mmWave signals (i.e., above 30 GHz) for communication purposes have created great interest from the perspective of localization, mapping, and simultaneous localization and mapping (SLAM) [1]–[3]. In both IEEE WLAN [4] and 3GPP cellular systems [5], this interest is motivated by the high resolution offered in delay (by virtue of large bandwidths) and angle (thanks to electrically large arrays) [6]. In turn, this has led to intense research activities in these areas [6]. With the focus now on 6G, integrated sensing and communication (ISAC) leverages these same properties in order to fundamentally integrate sensing (which includes positioning, mapping, and SLAM) into the communication system [7]–[9].

Conventionally, positioning relies on the line-of-sight (LoS) path between a user equipment (UE) and several base stations (BSs), while mapping harnesses the non-line-of-sight (NLoS) paths, resulting from scattering and reflection caused by objects in the environment [1], [10]. To reduce the reliance on multiple BSs, single-BS positioning and mapping has gathered significant interest [1], [3], [11], [12]. In this case, the UE combines information from the LoS and NLoS paths between itself and a single BS in order to determine its own position and locate the objects in the environment [10]. An important caveat here is that these works typically assume that all NLoS paths are so-called *single-bounce paths*, meaning that they correspond to a single discrete interaction point (IP) in the environment. This assumption is motivated by the large path loss at mmWave bands, making higher-order bounces less likely. However, measurements indicate that higher-order NLoS paths are not uncommon [1], [2], [13], [14]. Incorrectly using such paths as single-bounce paths can lead to severe positioning and mapping errors [11], [15]. To address higher-order NLoS bounce paths, several approaches have been considered in the literature. These can be categorized into either (i) classify and discard [2], [11], [15] or (ii) classify and exploit [13], [14]. The first category inherits from the classical single-bounce NLoS classification literature [2], [16], and aims to separate the higher-order bounces from the LoS and single-bounce paths, by relying on features of the paths such as signal power or spatial consistency. The second category inherits from the multi-path exploitation literature and has so-far been limited to perfect reflections [13], [14], where higher-order interactions can be determined via so-called virtual anchors.

In this paper, we follow the latter track and consider the multi-bounce paths as informative rather than a disturbance. Building on our previous work [11], where we proposed to separate the multi-bounce paths from LoS and single-bounce paths using a RANSAC-like approach, we devise a novel method that reveals that properly using second-order interactions can allow us to discover *new landmarks that were not visible from the single-order interactions*. Our specific contributions are: (i) a method that uses the estimated UE location and map from single-bounce interactions to determine likely second-order bounces; (ii) for these second-order bounces, a novel method is proposed to determine the two IPs using the geometric channel measurements; (iii) the proposed methods are validated using experimental mmWave data using 5G waveforms, demonstrating the ability to identify new landmarks.

II. Problem Formulation

We consider a bistatic downlink scenario with a single BS and a single UE. Although our focus is on the 2D/azimuth domain (position $\mathbf{p} = [x, y]^\top$ and orientation angle α) to simplify the notation, the extension to 3D is possible (conceptually similar to, e.g., [17]). The position and orientation of the BS is known and the state is given by $\mathbf{x}_{\mathrm{BS}} = [\mathbf{p}_{\mathrm{BS}}^\top, \alpha_{\mathrm{BS}}]^\top \in \mathbb{R}^3$. The UE state is unknown and given by $\mathbf{x}_{\mathrm{UE}} = [\mathbf{p}_{\mathrm{UE}}^\top, \alpha_{\mathrm{UE}}, b_{\mathrm{UE}}]^\top \in \mathbb{R}^4$ in which b_{UE} denotes the clock error between the UE and BS clock. The nth landmark is represented by position $\mathbf{p}_n \in \mathbb{R}^2$. Based on a standard channel parameter estimation method (see, e.g., [1], [2]), for each resolvable propagation path i we obtain as estimate of the time-of-arrival (ToA) τ_i, azimuth angle of angle-of-departure (AoD) ϕ_i, and angle-of-arrival (AoA) θ_i. The channel parameter estimate of the ith path is denoted by the tuple $\mathbf{z}_i = [\tau_i, \phi_i, \theta_i]^\top$ and the set of N tuples by the set

This work has been supported by the Academy of Finland (grants #338224, #345654, #352754 and #359095), by Business Finland (6G-ISAC project), and by the Vinnova B5GPOS Project under Grant 2022-01640. Email: {ossi.kaltiokallio, jukka.talvitie, elizaveta.rastorgueva-foi, mikko.valkama}@tuni.fi, {yuge,henkw}@chalmers.se

$\mathcal{Z} = \{\mathbf{z}_1, \dots, \mathbf{z}_N\}$. The unknowns $\mathbf{x}_{\text{UE}}$ and $\mathbf{p}_n$'s are estimated by SLAM using the information provided by $\mathcal{Z}$. This paper aims to utilize the SLAM solution for mapping second-order interactions that allows us to discover new landmarks that were not visible from the single-order interactions. Note that the elements in $\mathcal{Z}$ are unordered and, for each propagation path i, it is unknown whether it is LoS, single-bounce NLoS, or multi-bounce NLoS.

A. Geometric Measurement Model

Let us denote the IPs of an m-bounce signal of the ith path using set $\mathcal{P}_i^{\text{IP}} = \{\mathbf{p}_i^1, \mathbf{p}_i^2, \dots, \mathbf{p}_i^m\}$ with random cardinality and random elements. Assuming that the measurement noise is zero-mean Gaussian, the likelihood function is given by

$$p(\mathbf{z}_i \mid \mathbf{x}_{\text{UE}}, \mathcal{P}_i^{\text{IP}}) = \mathcal{N}(\mathbf{z}_i \mid \mathbf{h}_i(\mathbf{x}_{\text{UE}}, \mathcal{P}_i^{\text{IP}}), \mathbf{R}_i), \tag{1}$$

with covariance $\mathbf{R}_i$, and the mean $\mathbf{h}_i(\mathbf{x}_{\text{UE}}, \mathcal{P}_i^{\text{IP}})$ is given by

$$\mathbf{h}_i(\mathbf{x}_{\text{UE}}, \mathcal{P}_i^{\text{IP}}) = \begin{bmatrix} d_i/c + b_{\text{UE}} \\ \text{atan2}(-\delta_i^{1,y}, -\delta_i^{1,x}) - \alpha_{\text{BS}} \\ \text{atan2}(\delta_i^{2,y}, \delta_i^{2,x}) - \alpha_{\text{UE}} \end{bmatrix}, \tag{2}$$

which represents the geometric relationship between the BS, UE and $\mathcal{P}_i^{\text{IP}}$. In (2), c is the speed of light. Parameters of the model for the LoS and NLoS paths are defined as:

- *LoS* – The signal propagates directly from BS to UE such that $\mathcal{P}_i^{\text{IP}} = \varnothing$ and the parameters of (2) are:

$$d_i = \|\mathbf{p}_{\text{BS}} - \mathbf{p}_{\text{UE}}\|, \tag{3}$$

$$[\delta_i^{1,x}, \delta_i^{1,y}]^\top = [\delta_i^{2,x}, \delta_i^{2,y}]^\top = \mathbf{p}_{\text{BS}} - \mathbf{p}_{\text{UE}}, \tag{4}$$

  where $\|\cdot\|$ denotes the Euclidean norm;
- *NLoS* – The signal experiences m interactions with the environment as it propagates from the BS to the UE such that $\mathcal{P}_i^{\text{IP}} = \{\mathbf{p}_i^1, \mathbf{p}_i^2, \dots, \mathbf{p}_i^m\}$. The parameters of (2) are:

$$d_i = \|\mathbf{p}_{\text{BS}} - \mathbf{p}_i^1\| + \|\mathbf{p}_i^m - \mathbf{p}_{\text{UE}}\| + \textstyle\sum_{j=1}^{m-1} \|\mathbf{p}_i^{j+1} - \mathbf{p}_i^j\|, \tag{5}$$

$$[\delta_i^{1,x}, \delta_i^{1,y}]^\top = \mathbf{p}_{\text{BS}} - \mathbf{p}_i^1, \tag{6}$$

$$[\delta_i^{2,x}, \delta_i^{2,y}]^\top = \mathbf{p}_i^m - \mathbf{p}_{\text{UE}}, \tag{7}$$

  where we have assumed that $\mathbf{p}_i^1$ is the first IP after transmission and $\mathbf{p}_i^m$ is the last IP before reception. Note that if $\mathcal{P}_i^{\text{IP}} = \{\mathbf{p}_i^1\}$, $\mathbf{p}_i^m = \mathbf{p}_i^1$ and the model reduces to a conventional single-bounce model [1], [3], [11], [12].

B. Snapshot SLAM

We can express the UE position with respect to the BS using any measurement $\mathbf{z}_i$ as follows. The AoD and AoA for a single path can be represented by unit vectors $\mathbf{u}_i$ and $\mathbf{v}_i$, given by

$$\mathbf{u}_i = \mathbf{R}(\alpha_{\text{BS}}) \begin{bmatrix}\cos(\phi_i) & \sin(\phi_i)\end{bmatrix}^\top, \tag{8}$$

$$\mathbf{v}_i = \mathbf{R}(\alpha_{\text{UE}}) \begin{bmatrix}\cos(\theta_i) & \sin(\theta_i)\end{bmatrix}^\top, \tag{9}$$

in which $\mathbf{R}(\alpha)$ is a counterclockwise rotation matrix. Now using $\mathbf{u}_i$ and $\mathbf{v}_i$, the UE position is given by:

$$\mathbf{p}_{\text{UE}} = \mathbf{p}_{\text{BS}} + d_i\gamma_i^1\mathbf{u}_i - d_i\gamma_i^m\mathbf{v}_i + \textstyle\sum_{j=1}^{m-1}(\mathbf{p}_i^{j+1} - \mathbf{p}_i^j), \tag{10}$$

where $\gamma_i^1 \in [0,1]$ and $\gamma_i^m \in [0,1]$ are unknown and they represent the fraction of the propagation distance along $\mathbf{u}_i$ and $\mathbf{v}_i$, respectively, and $\gamma_i^1 + \gamma_i^m \le 1$. Since the terms in the sum are unknown, (10) does not admit a unique solution and therefore, exploiting multi-bounce signals for SLAM is very challenging. Moreover, multi-bounce signals will cause significant SLAM performance degradation since the multi-bounce and single-bounce models have a mismatch. To overcome this deficit, two recent works have explored methods to identify multi-bounce signals so that these paths can be excluded from $\mathcal{Z}$ when solving the SLAM problem [11], [15]. Let $\mathcal{I}$ denote the set of indices of $\mathcal{Z}$ that either correspond to the LoS or single-bounce NLoS path. Now for $i \in \mathcal{I}$, (10) simplifies to [17]

$$\mathbf{p}_{\text{UE}} = \mathbf{p}_{\text{BS}} + d_i\gamma_i\mathbf{u}_i - d_i(1-\gamma_i)\mathbf{v}_i, \tag{11}$$

in which $\gamma_i \in [0,1]$ for single-bounce and $\gamma_i = 1$ for LoS. From (11), a solution for the UE position can be derived [11], [18]: let $\mathbf{x} = [\mathbf{p}_{\text{UE}}^\top, b_{\text{UE}}]^\top$ and introduce the costs $J_i(\mathbf{x}, \alpha_{\text{UE}}) = \|\mathbf{H}_i\mathbf{x} - \boldsymbol{\mu}_i - \boldsymbol{\nu}_i^\top(\mathbf{H}_i\mathbf{x} - \boldsymbol{\mu}_i)\boldsymbol{\nu}_i\|^2$ and $J(\mathbf{x}, \alpha_{\text{UE}}) = \sum_{i\in\mathcal{I}} \eta_i J_i(\mathbf{x}, \alpha_{\text{UE}})$, where η_i is the weight of path i, $\mathbf{H}_i = [\mathbf{I}_{2\times2}, -c\mathbf{v}_i]$, $\mathbf{C}_i = \mathbf{I}_{2\times2} - \boldsymbol{\nu}_i\boldsymbol{\nu}_i^\top$, $\boldsymbol{\nu}_i = (\mathbf{u}_i + \mathbf{v}_i)/\|\mathbf{u}_i + \mathbf{v}_i\|$ and $\boldsymbol{\mu}_i = \mathbf{p}_{\text{BS}} - c\tau_i\mathbf{v}_i$. Conditional on α_{UE} (and thus on $\mathbf{v}_i$), $J(\mathbf{x}, \alpha_{\text{UE}})$ can be minimized with respect to $\mathbf{x}$ as

$$\hat{\mathbf{x}}(\alpha_{\text{UE}}) = \left(\textstyle\sum_{i\in\mathcal{I}} \eta_i\mathbf{H}_i^\top\mathbf{C}_i\mathbf{H}_i\right)^{-1} \textstyle\sum_{i\in\mathcal{I}} \eta_i\mathbf{H}_i^\top\mathbf{C}_i\boldsymbol{\mu}_i, \tag{12}$$

after which α_{UE} is the mimimizer of $J(\hat{\mathbf{x}}(\alpha_{\text{UE}}), \alpha_{\text{UE}})$.

1) Robust Estimator for Snapshot SLAM: The work in [11] introduced an algorithm that can find the inlier set $\mathcal{I}$, which corresponds to indices of $\mathcal{Z}$ that either originate from LoS or single-bounce NLoS paths. Let N_{min} denote the minimum number of channel parameter estimates required to solve (12) and let $\mathcal{J} \in \mathbb{R}^{L\times N_{\text{min}}}$ denote all L such possible combinations of the indices of $\mathcal{Z}$. In essence, the robust snapshot SLAM method first uses $\mathcal{I} \in \mathcal{J}$ to compute an initial solution. Then, according to the principles of RANSAC, the channel parameter estimates are partitioned into a set of inliers $\mathcal{I}_{\text{inliers}}$ and a set of outliers $\mathcal{I}_{\text{outliers}}$ based on the initial solution. Lastly, the problem is re-solved using (12) and the inlier set ($\mathcal{I} \leftarrow \mathcal{I}_{\text{inliers}}$), and a cost for the solution is computed as [11] $C(\alpha_{\text{UE}}, \mathcal{I}) = \sum_{i\in\mathcal{I}} \eta_i J_i(\hat{\mathbf{x}}(\alpha_{\text{UE}}), \alpha_{\text{UE}}) + \sum_{i\notin\mathcal{I}} \eta_i T_\varepsilon$, where T_ε is a constant penalty term for the outliers. The algorithm performs the above three steps for all possible combinations $\mathcal{J}$ and UE orientations $\mathcal{A}$. Then, the UE state estimate $\hat{\mathbf{x}}_{\text{UE}} = [\hat{\mathbf{p}}_{\text{UE}}^\top, \hat{\alpha}_{\text{UE}}, \hat{b}_{\text{UE}}]^\top$ and set of inliers $\hat{\mathcal{I}}$ is found as

$$\underset{\alpha_{\text{UE}}\in\mathcal{A}, \mathcal{I}\in\mathcal{J}}{\text{minimize}}\; C(\alpha_{\text{UE}}, \mathcal{I}), \tag{13}$$

and $\hat{\mathbf{p}}_{\text{UE}}$ and $\hat{b}_{\text{UE}}$ are given in closed-form when solving (13). After solving $\hat{\mathbf{x}}_{\text{UE}}$ and for every element of the inlier set $n \in \hat{\mathcal{I}}$, $\hat{\mathbf{p}}_n$ can be estimated independently by solving a nonlinear optimization problem as presented in [11]. Landmark n is an element of a first-order interactions map $\mathcal{M}_{\text{FO}}$, given by $\hat{\mathcal{M}}_{\text{FO}} = \{\hat{\mathbf{p}}_1, \dots, \hat{\mathbf{p}}_{|\hat{\mathcal{I}}|}\}$. In addition, an estimated propagation path is constructed as $\hat{\mathcal{P}}_n = \{\mathbf{p}_{\text{BS}}, \hat{\mathbf{p}}_n, \hat{\mathbf{p}}_{\text{UE}}\}$, and the set of first-order propagation paths is given by $\hat{\mathcal{P}}_{\text{FO}} = \{\hat{\mathcal{P}}_1, \dots, \hat{\mathcal{P}}_{|\hat{\mathcal{I}}|}\}$.

III. Mapping with Double-bounce Signals

A. Estimating Second-order Interaction Point

In this section, the estimated map $\hat{\mathcal{M}}_{\text{FO}}$, estimated UE state $\hat{\mathbf{x}}_{\text{UE}}$ and estimated outliers $i \notin \hat{\mathcal{I}}$ are used to estimate IPs of double-bounce propagation paths. Let $i \notin \hat{\mathcal{I}}$ denote the considered measurement $\mathbf{z}_i = [\tau_i, \phi_i, \theta_i]^\top$ and (assuming

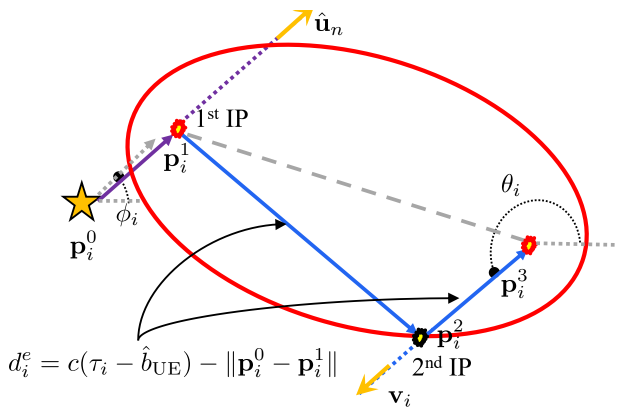

Fig. 1. Illustrative demonstration of the proposed closed-form solution to estimate $\mathbf{p}_i^2$. We consider a case where $\mathbf{p}_i^0$ represents the BS and $\mathbf{p}_i^3$ represents the UE. The closed-form solution to $\mathbf{p}_i^2$ is the intersection point between the half line, which starts from $\mathbf{p}_i^3$ alongside the direction $\mathbf{v}_i$, and the ellipse, which is determined by distance d_i^e and the two foci at $\mathbf{p}_i^1$ and $\mathbf{p}_i^3$. All the other landmarks are omitted for simplification.

double-bounce propagation) let $\mathcal{P}_i = \{\mathbf{p}_i^0, \mathbf{p}_i^1, \mathbf{p}_i^2, \mathbf{p}_i^3\}$ denote the starting point, two IPs and the end point of path i. Here, $\mathcal{P}_i$ is parameterized by two unknown IPs, $\mathbf{p}_i^1 \in \mathbb{R}^2$ and $\mathbf{p}_i^2 \in \mathbb{R}^2$, and since each propagation path only has three known channel parameters, the problem is underdetermined, i.e., the range of feasible solutions for the IPs is unbounded. To make the problem tractable, we aim to identify an element of $\hat{\mathcal{M}}_{\mathrm{FO}}$ as $\mathbf{p}_i^1$ and then solve for $\mathbf{p}_i^2$.

Let $\mathbf{\Psi} = [\Delta\hat{\phi}_1, \ldots, \Delta\hat{\phi}_{|\mathcal{M}_{\mathrm{FO}}|}, \Delta\hat{\theta}_1, \ldots, \Delta\hat{\theta}_{|\mathcal{M}_{\mathrm{FO}}|}]^\top$ denote the difference between the estimated and reconstructed angles, with elements corresponding to the nth landmark $\hat{\mathbf{p}}_n$ defined as $\Delta\hat{\phi}_n = \mathrm{acos}(\hat{\mathbf{u}}_n \cdot \mathbf{u}_i)$ and $\Delta\hat{\theta}_n = \mathrm{acos}(\hat{\mathbf{v}}_n \cdot \mathbf{v}_i)$, where $\hat{\mathbf{u}}_n = (\hat{\mathbf{p}}_n - \mathbf{p}_{\mathrm{BS}})/\|\hat{\mathbf{p}}_n - \mathbf{p}_{\mathrm{BS}}\|$, $\hat{\mathbf{v}}_n = (\hat{\mathbf{p}}_n - \hat{\mathbf{p}}_{\mathrm{UE}})/\|\hat{\mathbf{p}}_n - \mathbf{p}_{\mathrm{UE}}\|$, $\mathbf{u}_i$ is given by (8) and $\mathbf{v}_i$ is given by (9). To avoid error propagation, we retain only entries satisfying $[\mathbf{\Psi}]_n < \sigma_{\mathbf{\Psi}}$, allowing us to determine the first IP as

$$\mathbf{p}_i^1 = \hat{\mathbf{p}}_{n \bmod |\mathcal{M}_{\mathrm{FO}}|}, \quad \text{where} \quad n = \arg\min_n [\mathbf{\Psi}]_n. \tag{14}$$

If $n \le |\mathcal{M}_{\mathrm{FO}}|$, the sequence of signal interactions is BS $\to \mathbf{p}_i^1 \to \mathbf{p}_i^2 \to$ UE, such that $\mathbf{p}_i^0 = \mathbf{p}_{\mathrm{BS}}$, $\mathbf{p}_i^3 = \hat{\mathbf{p}}_{\mathrm{UE}}$. On the other hand if $n > |\mathcal{M}_{\mathrm{FO}}|$, we consider the signal interactions in reverse order UE $\to \mathbf{p}_i^1 \to \mathbf{p}_i^2 \to$ BS, such that $\mathbf{p}_i^0 = \hat{\mathbf{p}}_{\mathrm{UE}}$ and $\mathbf{p}_i^3 = \mathbf{p}_{\mathrm{BS}}$.

Now we will determine $\mathbf{p}_i^2$. If $n \le |\mathcal{M}_{\mathrm{FO}}|$, $\mathbf{p}_i^2$ locates on a line defined by $\mathbf{t}_i$ that spans from the UE toward the AoA and we set $\mathbf{t}_i = \mathbf{v}_i$ from (9). If $n > |\mathcal{M}_{\mathrm{FO}}|$, $\mathbf{p}_i^2$ locates on a line that spans from the BS toward the AoD and we define $\mathbf{t}_i = \mathbf{u}_i$ from (8). In either case, $\mathbf{p}_i^2$ can now be obtained by solving

$$\begin{cases} \|\mathbf{p}_i^2 - \mathbf{p}_i^1\| + \|\mathbf{p}_i^2 - \mathbf{p}_i^3\| = d_i^e, \\ (\mathbf{p}_i^2 - \mathbf{p}_i^3)\mathbf{t}_i^\top = \|\mathbf{p}_i^2 - \mathbf{p}_i^3\|. \end{cases} \tag{15}$$

The first entry in (15) indicates that $\mathbf{p}_i^2$ resides on an ellipse, with $\mathbf{p}_i^1$ and $\mathbf{p}_i^3$ as foci, where $d_i^e = c(\tau_i - \hat{b}_{\mathrm{UE}}) - \|\mathbf{p}_i^0 - \mathbf{p}_i^1\|$. The second entry in (15) indicates that $\mathbf{p}_i^2$ lies on a half line which starts from $\mathbf{p}_i^3$ alongside the direction of $\mathbf{t}_i$. A closed-form solution of (15) exists, but the derivation is omitted for brevity. Fig. 1 provides an illustrative representation of the proposed method to estimate $\hat{\mathbf{p}}_i^2$. Interaction point $\hat{\mathbf{p}}_i^2$ is an element of a second-order interactions map $\mathcal{M}_{\mathrm{SO}}$, given by

Algorithm 1 Proposed mapping algorithm

1: Set $\hat{\mathcal{M}}_{\mathrm{FO}} = \varnothing$, $\hat{\mathcal{P}}_{\mathrm{FO}} = \varnothing$, $\hat{\mathcal{M}}_{\mathrm{SO}} = \varnothing$ and $\hat{\mathcal{P}}_{\mathrm{SO}} = \varnothing$
2: **for** $k = 1, \ldots, K$ **do** `%Estimate 1st-order map`
3:     Compute $\hat{\mathbf{x}}_k^{\mathrm{UE}}$ and $\hat{\mathcal{I}}_k$ using (13) and $\mathcal{Z}_k$
4:     $\forall i \in \hat{\mathcal{I}}_k$, compute $\hat{\mathbf{p}}_i$ and $\hat{\mathcal{P}}_i$ and append to $\hat{\mathcal{M}}_{\mathrm{FO}} = \hat{\mathcal{M}}_{\mathrm{FO}} \cup \hat{\mathbf{p}}_i$ and $\hat{\mathcal{P}}_{\mathrm{FO}} = \hat{\mathcal{P}}_{\mathrm{FO}} \cup \hat{\mathcal{P}}_i$
5: **end for**
6: **for** $k = 1, \ldots, K$ **do** `%Estimate 2nd-order map`
7:     Using $\hat{\mathbf{x}}_k^{\mathrm{UE}}$, $\mathcal{Z}_k$, $\hat{\mathcal{M}}_{\mathrm{FO}}$, compute $\hat{\mathbf{p}}_i^2$ and $\hat{\mathcal{P}}_i$ $\forall i \notin \hat{\mathcal{I}}_k$ using (15) and append to $\hat{\mathcal{M}}_{\mathrm{SO}} = \hat{\mathcal{M}}_{\mathrm{SO}} \cup \hat{\mathbf{p}}_i^2$ and $\hat{\mathcal{P}}_{\mathrm{SO}} = \hat{\mathcal{P}}_{\mathrm{SO}} \cup \hat{\mathcal{P}}_i$
8: **end for**
9: Set $\hat{\mathcal{M}} = \hat{\mathcal{M}}_{\mathrm{FO}} \cup \hat{\mathcal{M}}_{\mathrm{SO}}$ and $\hat{\mathcal{P}} = \hat{\mathcal{P}}_{\mathrm{FO}} \cup \hat{\mathcal{P}}_{\mathrm{SO}}$
10: $\forall \hat{\mathcal{P}}_i \in \hat{\mathcal{P}}$, **if** $\hat{\mathcal{P}}_i$ is infeasible **do** $\hat{\mathcal{M}} = \hat{\mathcal{M}} \setminus \{\hat{\mathbf{p}}_i\}$ and $\hat{\mathcal{P}} = \hat{\mathcal{P}} \setminus \hat{\mathcal{P}}_i$

$\hat{\mathcal{M}}_{\mathrm{SO}} = \{\hat{\mathbf{p}}_i^2 \mid i \notin \hat{\mathcal{I}}\}$. Respectively, the second-order propagation paths are constructed as $\hat{\mathcal{P}}_{\mathrm{SO}} = \{\hat{\mathcal{P}}_i \mid i \notin \hat{\mathcal{I}}\}$, in which $\hat{\mathcal{P}}_i$ denotes an estimate of $\mathcal{P}_i$.

B. Proposed Mapping Algorithm with Artefact Removal

Thus far, we have only considered a single UE location and the extension to multiple UE locations $\mathbf{x}_{1:K}^{\mathrm{UE}}$ is straightforward. For every UE location $\mathbf{x}_k^{\mathrm{UE}}$, the robust snapshot SLAM algorithm is run separately and the aggregated first-order interaction map is built. Then, using estimates of the robust snapshot SLAM algorithm and the first-order map, the second-order interaction map is built. The algorithm is summarized in Algorithm 1 and the final map and estimated propagation paths are denoted as $\hat{\mathcal{M}}$ and $\hat{\mathcal{P}}$, respectively. Details of the artefact removal method on line 10 of Algorithm 1 are presented in the following.

If a higher-order interaction is mapped using a lower-order propagation model, it is possible that the estimated landmark location does not correspond to an actual physical obstruction, which we refer to as a *ghost artefact* in the following. To identify and discard ghost artefacts, we devise a method based on occupancy grid maps. An occupancy grid map, $\mathbf{m}$, represents the map of the explored environment as a field of random variables $\mathbf{m}_j \in \mathbf{m}$, arranged in an evenly spaced grid [19]. Each random variable is binary and corresponds to the occupancy of the location it covers (the cell is occupied if $p(\mathbf{m}_j = 1) = 1$ and unobstructed if $p(\mathbf{m}_j = 1) = 0$). Assuming the cells are independent of each other, the map posterior can be approximated as the product of its marginals [20, Eq. 9.4]

$$p(\mathbf{m} \mid \mathbf{r}_{1:P}, \mathbf{s}_{1:P}) = \prod_j p(\mathbf{m}_j \mid \mathbf{r}_{1:P}, \mathbf{s}_{1:P}), \tag{16}$$

where $\mathbf{r}_{1:P}$ denotes the set of observations, $\mathbf{s}_{1:P}$ the sensor trajectory defined as the sequence of all poses, and $P = |\hat{\mathcal{P}}|$ the cardinality. In mobile robotics, $\mathbf{s}_{1:P}$ represents the robot poses and $\mathbf{r}_{1:P}$ are obtained for example using LIDAR. However, to utilize occupancy grid maps in bistatic radio SLAM requires transforming $\hat{\mathcal{P}}$ to a set of observations (angle and range) and poses (location). Let us consider propagation path $\hat{\mathcal{P}}_i \in \hat{\mathcal{P}}$ and let us assume $\hat{\mathcal{P}}_i$ is a propagation path with two IPs, $\hat{\mathcal{P}}_i = \{\mathbf{p}_i^0, \mathbf{p}_i^1, \mathbf{p}_i^2, \mathbf{p}_i^3\}$. Now, we define the sensor poses as $\mathbf{s}_i = [\mathbf{p}_i^0, \mathbf{p}_i^1, \mathbf{p}_i^3]$ and observations $\mathbf{r}_i = [\mathbf{r}_i^1, \mathbf{r}_i^2, \mathbf{r}_i^3]$ as

$$\mathbf{r}_i^1 = [\|\mathbf{p}_i^0 - \mathbf{p}_i^1\|, \mathrm{atan2}(y_i^1 - y_i^0, x_i^1 - x_i^0)]^\top, \tag{17}$$

$$\mathbf{r}_i^2 = [\|\mathbf{p}_i^1 - \mathbf{p}_i^2\|, \mathrm{atan2}(y_i^2 - y_i^1, x_i^2 - x_i^1)]^\top, \tag{18}$$

$$\mathbf{r}_i^3 = [\|\mathbf{p}_i^2 - \mathbf{p}_i^3\|, \mathrm{atan2}(y_i^2 - y_i^3, x_i^2 - x_i^3)]^\top. \tag{19}$$

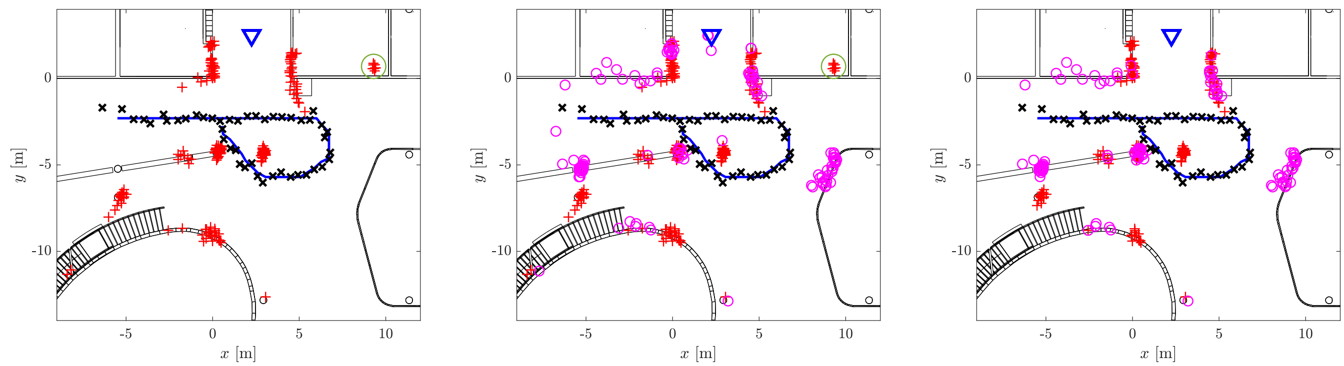

(a) SB map (b) SB and DB map (c) SB and DB map with artefact removal

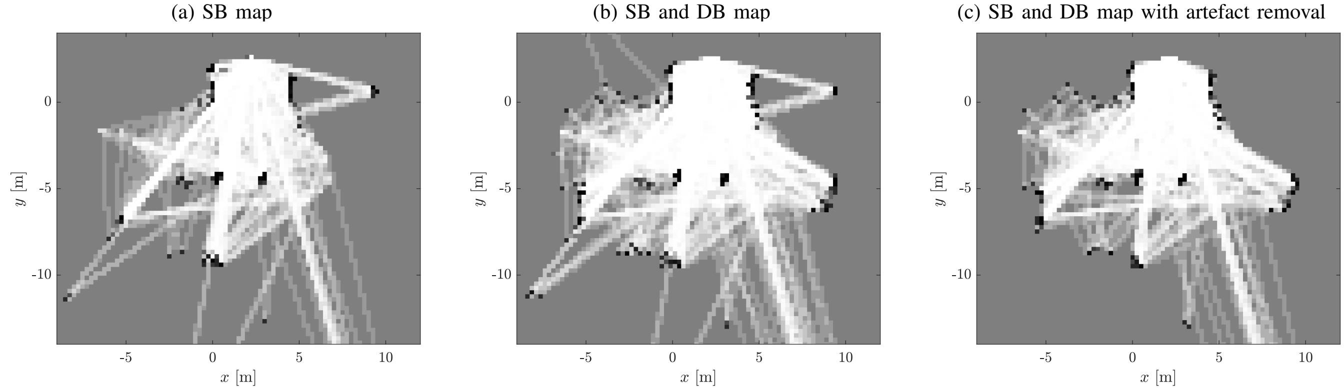

(d) SB occupancy map (e) SB and DB occupancy map (f) SB and DB occupancy map with artefact removal

Fig. 2. On the top row: (a) single-bounce (SB) method; (b) SB and double-bounce (DB) method; (c) SB and DB method with artefact removal. The legend of the figures is: BS (▽), ground truth UE locations (——), estimated UE locations (×), SB IPs (+) and DB IPs (○). On the bottom row, the occupancy maps of SB method in (d), SB and DB method in (e) and SB and DB with artefact removal method in (f). The color scale of the occupancy maps is: unoccupied cells (□), occupied cells (■) and unmapped cells (■). In (a) and (b), a ghost artefact caused by a triple-bounce signal is highlighted using a green circle at $\mathbf{p} \approx [9,\ 1]^\top$.

For a single-bounce path $\hat{\mathcal{P}}_i = \{\mathbf{p}_i^0, \mathbf{p}_i^1, \varnothing, \mathbf{p}_i^3\}$, $\mathbf{p}_i^2 = \mathbf{p}_i^1$ and the sensor poses and observations are defined as $\mathbf{s}_i = [\mathbf{p}_i^0, \mathbf{p}_i^3]$ and $\mathbf{r}_i = [\mathbf{r}_i^1, \mathbf{r}_i^3]$, respectively. After computing (16) as presented in [20, Ch. 9], for every $\hat{\mathcal{P}}_i \in \hat{\mathcal{P}}$ we check feasibility of the propagation path and if it is infeasible, we remove the ith element from $\hat{\mathcal{P}}$ and $\hat{\mathcal{M}}$ in accordance with line 10 of Algorithm 1. The path is infeasible if it propagates through obstacles —evaluated using the estimated occupancy grid map as follows. From $\mathbf{m}$ we compute $p(\mathbf{m}_j)$ for every cell $\mathbf{m}_j \in \mathbf{m}$ the estimated path $\hat{\mathcal{P}}_i$ traverses through and if $p(\mathbf{m}_j = 1) > 0.7$, the cell is occupied and $\hat{\mathcal{P}}_i$ is known to traverse through an obstacle such that the propagation path is physically unlikely. It is to be noted that close to elements of $\mathbf{p}_i \in \hat{\mathcal{P}}_i$, interaction with other estimated landmarks is likely and therefore, the occupancy of grid indices with $\|\mathbf{m}_j - \mathbf{p}_i\| < \sigma_{\mathbf{m}}$ are ignored.

IV. Experimental Results

A. Experimental Setup

The performance of the proposed double-bounce mapping algorithm is evaluated using real-world 60 GHz measurement data, obtained indoors at Tampere University campus, with floorplan as illustrated in Fig. 2. Altogether 45 UE locations were measured. Beamformed measurements were obtained using 400 MHz transmission bandwidth utilizing 5G NR-specified downlink positioning reference signals. Details of the experimental setup and used hardware are presented in [1]. In this paper, the AoD and AoA are estimated from the beam reference signal received power measurements using a constant false alarm rate-based detector and thereafter, the ToA is estimated as presented in [1]. The robust snapshot SLAM algorithm is implemented using the same parameters as presented in [11], the angle error threshold used in (14) is $\sigma_{\mathbf{\Psi}} = 1°$ and the artefact removal threshold is $\sigma_{\mathbf{m}} = 1$ m.

B. Mapping Results

Since the ground truth landmark locations are unknown, which is a common problem in SLAM when using real-world experimental data, we can only evaluate the UE state quantitatively, whereas mapping accuracy is evaluated visually by comparing the estimated map to the floor plan. The utilized robust snapshot radio SLAM algorithm yields good accuracy and the map created using the first-order interactions is on most parts in line with the floor plan of the experimental environment as illustrated in Fig. 2a. The position, heading and clock bias root mean squared error of the UE are: 0.29 m, 2.52° and 1.13 ns, respectively. The occupancy grid map is illustrated in Fig. 2d and it conveys important information. On most parts, the occupancy grid map is correct as occupied cells locate where actual obstructions exist and unoccupied cells depict unobstructed areas of the experimental environment. However, the occupancy grid map also indicates that there are several ghost artefacts corresponding to propagation paths that are physically impossible. For example at location $\mathbf{p} \approx [9, 1]^\top$, the occupancy grid map contains an obstruction and first-order interactions to this location propagate through a wall. In reality, the propagation path is a triple-bounce signal and the path traverses as follows: BS → right wall → left wall → right wall → UE. The angles of the triple-bounce signal matches the single-bounce model and therefore, the robust snapshot SLAM algorithm does not classify it as an outlier. Hence, it is possible that higher-order propagation paths are in line with the single-bounce model and as an outcome, such paths create ghost artefacts that do not physically correspond to an actual obstacle.

In the 45 UE locations, the robust snapshot SLAM algorithm classifies that the LoS exist in 32 UE locations, the total number of inliers is 234 and 147 of the channel parameter estimates are classified as outliers, possibly corresponding to second and higher-order interactions. The outliers constitute almost 40% of the channel parameter estimates and discarding them leads to a loss of valuable information. The map created using the assumed single and double-bounce propagation paths is illustrated in Fig. 2b and the occupancy grid map is shown in Fig. 2e. As illustrated, the IPs estimated using the proposed double-bounce mapping approach are in line with the floor plan of the experimental environment and the occupancy grid map is more informative than the single-bounce occupancy grid map. The main benefit of the proposed approach is that by properly using the second-order interactions can allow us to discover new IPs that were not visible from the single-order interactions. This follows directly from problem geometry. For example, the pillar located at $\mathbf{p} \approx [-6, -5.5]^\top$ and the walls located at $\mathbf{p} \approx [-9.5, -6]^\top$ and $\mathbf{p} \approx [-3, 0]^\top$ cannot be illuminated directly from the BS since the propagation path is obstructed. However, the features can be illuminated via other landmarks resulting in a double-bounce signal that can also provide valuable information about the surrounding environment as illustrated in the figures.

The downside of the double-bounce mapping approach is that the number of ghost artefacts in the estimated map increases. For example, there are several IPs in the unoccupied area (e.g. at $\mathbf{p} \approx [-7, -3]^\top$ and $\mathbf{p} \approx [2, 1.5]^\top$) and also one located at $\mathbf{p} \approx [-6, 6]^\top$ which is behind a wall. These artefacts either result from incorrectly estimating the first IP from the existing map or estimating higher-order interactions using the second-order model. Utilizing the artefact removal method presented in Section III-B allows us to identify propagation paths that are physically impossible such that they can be discarded from the map. As illustrated in Fig. 2c, the estimated map after artefact removal does not contain ghost artefacts and the occupancy grid map illustrated in Fig. 2f more accurately represents the experimental environment. After artefact removal, the total number of single-bounce and double-bounce paths is 198 and 113, respectively. Thus, the first-order interactions account for 52% of the NLoS measurements, whereas the first and second-order interactions explain 82% of the data, a notable increase in mapping information. The remaining 18% of the data contain the higher-order interactions and possible false detections of the channel estimator.

V. Conclusions

In this paper, a mapping algorithm using second-order interactions was devised. Using experimental mmWave measurements, it was demonstrated that it is possible to discover features of the environment that were not visible using single-order interactions —improving the generated maps, thus enhancing situational awareness. The newly proposed mapping algorithm admits numerous possibilities of future research into mapping with higher-order interactions and incorporating double and multi-bounce paths into SLAM.

References

[1] E. Rastorgueva-Foi *et al.*, “Millimeter-wave radio SLAM: End-to-end processing methods and experimental validation,” *IEEE J. Select. Areas Commun.*, pp. 1–1, 2024.

[2] C. Baquero Barneto *et al.*, “Millimeter-wave mobile sensing and environment mapping: Models, algorithms and validation,” *IEEE Trans. Veh. Technol.*, vol. 71, no. 4, pp. 3900–3916, 2022.

[3] Y. Ge *et al.*, “A computationally efficient EK-PMBM filter for bistatic mmWave radio SLAM,” *IEEE J. Select. Areas Commun.*, vol. 40, no. 7, pp. 2179–2192, 2022.

[4] A. Arun *et al.*, “P2SLAM: Bearing based WiFi SLAM for indoor robots,” *IEEE Robot. Autom. Lett.*, vol. 7, no. 2, pp. 3326–3333, 2022.

[5] H. Kim *et al.*, “PMBM-based SLAM filters in 5G mmWave vehicular networks,” *IEEE Trans. Veh. Technol.*, vol. 71, no. 8, pp. 8646–8661, 2022.

[6] B. Amjad *et al.*, “Radio SLAM: A review on radio-based simultaneous localization and mapping,” *IEEE Access*, vol. 11, pp. 9260–9278, 2023.

[7] C. De Lima *et al.*, “Convergent communication, sensing and localization in 6G systems: An overview of technologies, opportunities and challenges,” *IEEE Access*, vol. 9, pp. 26 902–26 925, 2021.

[8] A. Behravan *et al.*, “Positioning and sensing in 6G: Gaps, challenges, and opportunities,” *IEEE Veh. Technol. Mag.*, vol. 18, no. 1, pp. 40–48, 2023.

[9] Z. Wei *et al.*, “Integrated sensing and communication signals toward 5G-A and 6G: A survey,” *IEEE Internet Things J.*, vol. 10, no. 13, pp. 11 068–11 092, 2023.

[10] R. Mendrzik *et al.*, “Harnessing NLOS components for position and orientation estimation in 5G millimeter wave MIMO,” *IEEE Trans. Wireless Commun.*, vol. 18, no. 1, pp. 93–107, 2019.

[11] O. Kaltiokallio *et al.*, “Robust snapshot radio SLAM,” 2024. [Online]. Available: https://arxiv.org/abs/2404.10291

[12] M. A. Nazari *et al.*, “mmWave 6D radio localization with a snapshot observation from a single BS,” *IEEE Trans. Veh. Technol.*, vol. 72, no. 7, pp. 8914–8928, 2023.

[13] E. Leitinger *et al.*, “Data fusion for multipath-based SLAM: Combining information from multiple propagation paths,” *IEEE Trans. Signal Process.*, vol. 71, pp. 4011–4028, 2023.

[14] J. Kulmer *et al.*, “Anchorless cooperative tracking using multipath channel information,” *IEEE Trans. Wireless Commun.*, vol. 17, no. 4, pp. 2262–2275, 2018.

[15] Z. Li *et al.*, “An iterative 5G positioning and synchronization algorithm in NLOS environments with multi-bounce paths,” *IEEE Wireless Commun. Lett.*, vol. 12, no. 5, pp. 804–808, 2023.

[16] G. İsmail *et al.*, “NLOS identification and weighted least-squares localization for UWB systems using multipath channel statistics,” *EURASIP J. Advances Signal Process.*, vol. 2008, 12 2007.

[17] F. Wen *et al.*, “5G synchronization, positioning, and mapping from diffuse multipath,” *IEEE Wireless Commun. Lett.*, vol. 10, no. 1, pp. 43–47, 2021.

[18] Y. Ge *et al.*, “Experimental validation of single BS 5G mmWave positioning and mapping for intelligent transport,” *IEEE Trans. Veh. Technol.*, pp. 1–13, 2024.

[19] H. P. Moravec, “Sensor fusion in certainty grids for mobile robots,” *AI Magazine*, vol. 9, no. 2, p. 61, Jun. 1988.

[20] S. Thrun *et al.*, *Probabilistic Robotics (Intelligent Robotics and Autonomous Agents)*. The MIT Press, 2005.